

Pullback transformation in gyrokinetic electromagnetic simulations

Alexey Mishchenko*

Max Planck Institute for Plasma Physics, D-17491 Greifswald, Germany

Axel Könies, Ralf Kleiber, and Michael Cole

Max Planck Institute for Plasma Physics, D-17491 Greifswald, Germany

(Dated: July 15, 2018)

Abstract

It is shown that a considerable improvement in the global gyrokinetic electromagnetic simulations can be achieved by a slight modification of the simulation scheme. The new scheme is verified, simulating a Toroidal Alfvén Eigenmode in tokamak geometry at low perpendicular mode numbers, the so-called “MHD limit”. Also, an electromagnetic drift mode has been successfully simulated in a stellarator.

* alexey.mishchenko@ipp.mpg.de

I. INTRODUCTION

Electromagnetic effects, such as Alfvén waves or tearing dynamics, are of importance in fusion plasmas. A major complication for such simulations is caused by the so-called cancellation problem [1, 2]. This problem has been addressed by various authors both in the particle-in-cell (PIC) [2–5] and Eulerian [6] numerical framework. The scheme described in Refs. [2–6] is used by a number of numerical codes, but its performance may be inhibited, particularly when performing global simulations in realistic shaped geometries and at realistic plasma β values. Recently, an approach [7] has been suggested, based on a novel choice of the gyrokinetic variables, which makes it possible to mitigate the cancellation problem, in particular for Alfvénic-type dynamics where $E_{\parallel} \approx 0$. The drawback of this method is that it is limited to cases in which Alfvénic dynamics dominates. It does not help in the electromagnetic drift mode simulations and its performance diminishes considerably when diamagnetic drift effects become of importance, e.g. for the drift-kink instabilities. In this paper, we describe an algorithm overcoming such limitations.

We verify our scheme by simulating the Toroidal Alfvén Eigenmode (TAE) in tokamak geometry and the electromagnetic Ion Temperature Gradient-driven (ITG) mode in stellarator geometry. In tokamak geometry, we compare the results of the new scheme with previous simulations [7]. In stellarator geometry, we show that the simulations become feasible for the parameters considered only when the new scheme is applied. Otherwise, a severe numerical instability develops, caused by the cancellation problem.

The structure of the paper is as follows. In Sec. II the method suggested is described. In Sec. III the simulations verifying this method and demonstrating its performance are discussed. The conclusions are drawn in Sec. IV.

II. PULLBACK MITIGATION OF THE CANCELLATION PROBLEM

To derive the mitigation scheme, we deliberately split the magnetic potential into the ‘symplectic’ and ‘hamiltonian’ parts:

$$A_{\parallel} = A_{\parallel}^{(s)} + A_{\parallel}^{(h)} \tag{1}$$

This naming is inspired by Ref. [8]; the precise relation will become more clear in the following. In these notations, the perturbed guiding-center phase-space Lagrangian [8] is

$$\gamma = q\mathbf{A}^* \cdot d\mathbf{R} + \frac{m}{q}\mu d\theta + qA_{\parallel}^{(s)}\mathbf{b} \cdot d\mathbf{x} + qA_{\parallel}^{(h)}\mathbf{b} \cdot d\mathbf{x} - \left[\frac{mv_{\parallel}^2}{2} + \mu B + q\phi \right] dt \quad (2)$$

We now perform the Lie transform in such a way that the ‘hamiltonian part’ $A_{\parallel}^{(h)}$ contributes to the gyrokinetic Hamiltonian, whereas the ‘symplectic part’ $A_{\parallel}^{(s)}$ enters the gyrokinetic symplectic structure (this explains the naming employed). The resulting gyrokinetic phase-space Lagrangian is written to first order:

$$\Gamma = q\mathbf{A}^* \cdot d\mathbf{R} + \frac{m}{q}\mu d\theta + q\langle A_{\parallel}^{(s)} \rangle \cdot d\mathbf{R} - \left[\frac{mv_{\parallel}^2}{2} + \mu B + q\langle \phi - v_{\parallel}A_{\parallel}^{(h)} \rangle \right] dt \quad (3)$$

Here, $\langle \dots \rangle$ is the gyro-average, defined as usual. The formulation Eq. (3) is neither hamiltonian nor symplectic and will, therefore, be dubbed the ‘mixed-variable’ formulation, following Ref. [7]. The corresponding perturbed equations of motion are

$$\dot{\mathbf{R}}^{(1)} = \frac{\mathbf{b}}{B_{\parallel}^*} \times \nabla \langle \phi - v_{\parallel}A_{\parallel}^{(s)} - v_{\parallel}A_{\parallel}^{(h)} \rangle - \frac{q}{m} \langle A_{\parallel}^{(h)} \rangle \mathbf{b}^* \quad (4)$$

$$\dot{v}_{\parallel}^{(1)} = -\frac{q}{m} \left[\mathbf{b}^* \cdot \nabla \langle \phi - v_{\parallel}A_{\parallel}^{(h)} \rangle + \frac{\partial}{\partial t} \langle A_{\parallel}^{(s)} \rangle \right] - \frac{\mu}{m} \frac{\mathbf{b} \times \nabla B}{B_{\parallel}^*} \cdot \nabla \langle A_{\parallel}^{(s)} \rangle \quad (5)$$

For the scheme to work, an equation for $\partial A_{\parallel}^{(s)}/\partial t$ is needed. For example, one can follow Ref. [7] and use the ideal Ohm’s law, employing the definition:

$$\frac{\partial}{\partial t} A_{\parallel}^{(s)} + \mathbf{b} \cdot \nabla \phi = 0 \quad (6)$$

This approach appears to be most suitable for Alfvénic modes and is utilised throughout this paper. However, other equations for $\partial A_{\parallel}^{(s)}/\partial t$ can be considered, too. Such flexibility may be of interest for further optimisation of the simulation algorithm, but this is beyond the scope of the present paper.

The zeroth-order gyrocenter characteristics are as usual:

$$\dot{\mathbf{R}}^{(0)} = v_{\parallel}\mathbf{b}^* + \frac{1}{qB_{\parallel}^*}\mathbf{b} \times \mu\nabla B, \quad \dot{v}_{\parallel}^{(0)} = -\frac{\mu}{m}\mathbf{b}^* \cdot \nabla B \quad (7)$$

Here the following notation has been used:

$$B_{\parallel}^* = \mathbf{b} \cdot \tilde{\mathbf{B}}^*, \quad \tilde{\mathbf{B}}^* = \mathbf{B}^* + \nabla \langle A_{\parallel}^{(s)} \rangle \times \mathbf{b} \quad (8)$$

$$\mathbf{B}^* = \mathbf{B} + \frac{mv_{\parallel}}{q}\nabla \times \mathbf{b}, \quad \mathbf{b}^* = \mathbf{B}^*/B_{\parallel}^* \quad (9)$$

The mixed-variable distribution function is solved from the gyrokinetic Vlasov equation:

$$\frac{\partial f_{1s}^{(m)}}{\partial t} + \dot{\mathbf{R}}^{(0)} \cdot \frac{\partial f_{1s}^{(m)}}{\partial \mathbf{R}} + v_{\parallel}^{(0)} \frac{\partial f_{1s}^{(m)}}{\partial v_{\parallel}} = -\dot{\mathbf{R}}^{(1)} \cdot \frac{\partial F_{0s}}{\partial \mathbf{R}} - v_{\parallel}^{(1)} \frac{\partial F_{0s}}{\partial v_{\parallel}} \quad (10)$$

Here, the index $s = i, e, f$ denotes the particle species (ions, electrons, or fast ions); F_{0s} is the non-perturbed distribution function (usually a Maxwellian); the gyrocenter orbits are given by Eqs. (4), (5) and (7). In this paper, we apply the linearised version of the gyrokinetic equation, but the algorithm, described below, can also be used in nonlinear regime.

The electrostatic potential and the ‘hamiltonian part’ of the magnetic potential are found from the gyrokinetic quasineutrality equation and mixed-variable parallel Ampere’s law, respectively:

$$\int \frac{q_i F_{0i}}{T_i} (\phi - \langle \phi \rangle) \delta(\mathbf{R} + \boldsymbol{\rho} - \mathbf{x}) d^6 Z = \bar{n}_{1i} - \bar{n}_{1e} \quad (11)$$

$$\left(\frac{\beta_i}{\rho_i^2} + \frac{\beta_e}{\rho_e^2} - \nabla_{\perp}^2 \right) A_{\parallel}^{(h)} - \nabla_{\perp}^2 A_{\parallel}^{(s)} = \mu_0 (\bar{j}_{\parallel 1i} + \bar{j}_{\parallel 1e}) \quad (12)$$

with the usual notations: the mixed-variable gyrocenter density $\bar{n}_{1s} = \int d^6 Z f_{1s}^{(m)} \delta(\mathbf{R} + \boldsymbol{\rho} - \mathbf{x})$, whose relation to the physical density depends on the particular formulation of the gyrokinetic theory used; the mixed-variable gyrocenter current $\bar{j}_{\parallel 1s} = q_s \int d^6 Z f_{1s}^{(m)} v_{\parallel} \delta(\mathbf{R} + \boldsymbol{\rho} - \mathbf{x})$, related to the physical current by the pullback; the particle charge q_s ; the gyrokinetic phase-space volume $d^6 Z = B_{\parallel}^* d\mathbf{R} dv_{\parallel} d\mu d\theta$; the thermal gyroradius $\rho_s = \sqrt{m_s T_s / (eB)}$ and $\beta_s = \mu_0 n_0 T_s / B_0^2$.

Now, we consider how the mixed-variable formalism can be used in order to mitigate the cancellation problem. This problem appears in the conventional hamiltonian formulation of the gyrokinetic theory. In this formalism, the ‘parallel velocity’ variable is defined as

$$v_{\parallel}^{(h)} = v_{\parallel}^{(\text{gc})} + \frac{\mathbf{b}^*}{B} \cdot \nabla \left[\int^{\theta_{(\text{gc})}} (\psi - \langle \psi \rangle) d\theta_{(\text{gc})} \right] + \frac{e}{m} A_{\parallel}, \quad \psi = \phi - v_{\parallel}^{(\text{gc})} A_{\parallel} \quad (13)$$

Here, $v_{\parallel}^{(\text{gc})}$ is the usual guiding-center parallel velocity and $\theta_{(\text{gc})}$ is the guiding-center gyro-phase. The cancellation problem can be related to the last term $(e/m) A_{\parallel}$ in this definition. In contrast, this term is modified and the cancellation problem is absent in the symplectic formulation, with the ‘parallel velocity’

$$v_{\parallel}^{(s)} = v_{\parallel}^{(\text{gc})} + \frac{\mathbf{b}^*}{B} \cdot \nabla \left[\int^{\theta_{(\text{gc})}} (\psi - \langle \psi \rangle) d\theta_{(\text{gc})} \right] + \frac{e}{m} \tilde{A}_{\parallel}, \quad \tilde{A}_{\parallel} = A_{\parallel} - \langle A_{\parallel} \rangle \quad (14)$$

The mixed-variable formulation is intermediate between the hamiltonian and the symplectic formulations, with the ‘parallel velocity’ variable defined as

$$v_{\parallel}^{(m)} = v_{\parallel}^{(gc)} + \frac{\mathbf{b}^*}{B} \cdot \nabla \left[\int^{\theta_{(gc)}} (\psi - \langle \psi \rangle) d\theta_{(gc)} \right] + \frac{e}{m} A_{\parallel}^{(h)} + \frac{e}{m} \tilde{A}_{\parallel}^{(s)}, \quad \tilde{A}_{\parallel}^{(s)} = A_{\parallel}^{(s)} - \langle A_{\parallel}^{(s)} \rangle \quad (15)$$

The cancellation problem is still present in this formulation but it can be mitigated by minimising $A_{\parallel}^{(h)}$, which in contrast to A_{\parallel} is an arbitrarily chosen quantity. Note that the mixed-variable formulation becomes identical to the symplectic when $A_{\parallel}^{(h)} = 0$.

Invoking the pullback transformation [8], one can express the distribution function in the symplectic formulation through the mixed-variable distribution function as follows:

$$f_{1s}^{(s)} = f_{1s}^{(m)} + \frac{q_s \langle A_{\parallel}^{(h)} \rangle}{m_s} \frac{\partial F_{0s}}{\partial v_{\parallel}} \quad (16)$$

This equation results from the scalar nature of the distribution function, which implies $f_s^{(s)}[v_{\parallel}^{(s)}] = f_s^{(m)}[v_{\parallel}^{(m)}]$ for the total distribution functions $f_s^{(s)} = F_{0s} + f_{1s}^{(s)}$ and $f_s^{(m)} = F_{0s} + f_{1s}^{(m)}$. Here again one sees that the cancellation problem, absent in the symplectic formulation, can be greatly mitigated by minimising the difference $|f_{1s}^{(m)} - f_{1s}^{(s)}|$, or, equivalently, keeping the dominant part of the parallel vector potential in its ‘symplectic part’ $A_{\parallel} \approx A_{\parallel}^{(s)}$ which results in

$$A_{\parallel}^{(h)} \ll A_{\parallel} \quad (17)$$

In some cases, this can be achieved utilising certain ideas about the physical properties of the system under consideration, such as a particular form of Ohm’s law which can be used to determine the physically dominant part of the magnetic potential [7]. An alternative to this approach is to numerically accumulate the value of the magnetic potential in its symplectic part. For this purpose, we can modify the usual algorithm as follows.

1. At the end of each time step, redefine the magnetic potential splitting, Eq. (1), so that the entire instantaneous value of the parallel magnetic potential $A_{\parallel}(t_i)$ is collected in its ‘symplectic part’:

$$A_{\parallel(\text{new})}^{(s)}(t_i) = A_{\parallel}(t_i) = A_{\parallel(\text{old})}^{(s)}(t_i) + A_{\parallel(\text{old})}^{(h)}(t_i) \quad (18)$$

2. As a consequence of the new splitting, Eq. (18), the ‘hamiltonian’ part of the vector potential must be corrected:

$$A_{\parallel(\text{new})}^{(h)}(t_i) = 0 \quad (19)$$

3. For this modified splitting, the new mixed-variable distribution function must coincide with its symplectic-formulation counterpart. The symplectic-formulation distribution function is independent on the way of splitting and can be found invoking the pullback, Eq. (16), and using the old values of the mixed-variable distribution function and the ‘hamiltonian’ part of the parallel vector potential found solving, respectively, the gyrokinetic equation (10) and Ampere’s law, Eq. (12), at the current time step t_i :

$$f_{1s(\text{new})}^{(m)}(t_i) = f_{1s}^{(s)}(t_i) = f_{1s(\text{old})}^{(m)}(t_i) + \frac{q_s \langle A_{\parallel(\text{old})}^{(h)}(t_i) \rangle}{m_s} \frac{\partial F_{0s}}{\partial v_{\parallel}} \quad (20)$$

4. Proceed, explicitly solving the mixed-variable system of equations (4)-(12) at the next time step $t_i + \Delta t$ in a usual way, but using Eqs. (18)-(20) as the initial conditions.

This rearrangement between the symplectic and the hamiltonian components of the ‘initial conditions’ has to be done regularly, i.e. at each time step. Note that the parallel physics is determined by the time derivative of the magnetic potential, whereas the cancellation problem is proportional to its instantaneous value. In our approach, we force the ‘symplectic part’ $A_{\parallel}^{(s)}$ to be a dominant contribution to this value. The small residual $A_{\parallel}^{(h)}$ is self-consistently computed at each time step from the gyrokinetic system of equations in the mixed-variable formulation, thus guaranteeing correctness of the physical quantity $\partial A_{\parallel}/\partial t$, in accordance with the actual dynamics of the system. This ‘hamiltonian’ correction, being very small, will not lead to a cancellation problem of any significance. The scheme is not limited to Alfvénic systems, which obey $E_{\parallel} \approx 0$, and will work independently of the particular physical properties of the system considered. Since the key part of our approach, the distribution function transformation Eq. (20), is directly related to the pullback transform, Ref. [8], we call it the ‘pullback mitigation’ of the cancellation problem.

III. SIMULATIONS

In this section, we verify the scheme suggested above. We apply the particle-in-cell code EUTERPE [9], a non-axisymmetric extension of the GYGLES code [10–13], in tokamak and stellarator geometries. For consistency, we give here a short description of the numerical scheme used (also described elsewhere [9]).

The code solves the gyrokinetic equation using the characteristics Eqs. (4), (5) and (7). The perturbed fields ϕ , $A_{\parallel}^{(h)}$ and $A_{\parallel}^{(s)}$ are found numerically solving the quasineutrality

equation (11), parallel Ampère's law, Eq. (12), and parallel Ohm's law, Eq. (6). Here, the first two equations (11) and (12) represent boundary-value problems whereas the last one, Eq. (6), is an initial value-problem. We choose $A_{\parallel}^{(s)}(t=0) = 0$ as the initial condition for Ohm's law. The perturbed part of the distribution function is discretised with markers:

$$f_{1s}^{(m)}(\mathbf{R}, v_{\parallel}, \mu, t) = \sum_{\nu=1}^{N_p} w_{s\nu}(t) \delta(\mathbf{R} - \mathbf{R}_{\nu}) \delta(v_{\parallel} - v_{\nu\parallel}) \delta(\mu - \mu_{\nu}), \quad (21)$$

where N_p is the number of markers, $(\mathbf{R}_{\nu}, v_{\nu\parallel}, \mu_{\nu})$ are the marker phase space coordinates and $w_{s\nu}$ is the weight of a marker. The electrostatic and magnetic potentials are discretized with the finite-element method (Ritz-Galerkin scheme):

$$\phi(\mathbf{x}, t) = \sum_{l=1}^{N_s} \phi_l(t) \Lambda_l(\mathbf{x}), \quad A_{\parallel}^{(h)}(\mathbf{x}, t) = \sum_{l=1}^{N_s} a_l^{(h)}(t) \Lambda_l(\mathbf{x}), \quad A_{\parallel}^{(s)}(\mathbf{x}, t) = \sum_{l=1}^{N_s} a_l^{(s)}(t) \Lambda_l(\mathbf{x}), \quad (22)$$

where $\Lambda_l(\mathbf{x})$ are the finite elements (tensor product of B splines [14, 15]); N_s is the total number of the finite elements; ϕ_l , $a_l^{(h)}$ and $a_l^{(s)}$ are the spline coefficients. In this formulation, the gyrokinetic equation (10) corresponds to the evolution of the marker weights $w_{s\nu}(t)$ and the parallel Ohm's law, Eq. (6), translates into the evolution of the spline coefficients $a_l^{(s)}(t)$. A more detailed description of the discretization procedure can be found in Refs. [2, 4, 5, 16, 17]. We apply the so-called phase factor transform [16] to all perturbed quantities in the code. The integrals over the gyro-angle are approximated with an N-point discrete sum [17–19]. The cancellation problem [1, 2], which in the mixed-variable formulation is related only to the correction $A_{\parallel}^{(h)}$ of the parallel magnetic potential [see Eq. (12)], is solved using the iterative scheme introduced in Refs. [3, 5].

First, we consider a TAE in a tokamak configuration with a large aspect ratio and a circular cross section, the minor radius $r_a = 1$ m, the major radius $R_0 = 10$ m, the magnetic field on axis $B_0 = 3$ T, and the safety factor profile $q(r) = 1.71 + 0.16 (r/r_a)^2$ (here, r is the small radius). The background plasma profiles (corresponding to Maxwellian unperturbed distribution functions) are chosen to be flat with the ion (hydrogen) and electron densities $n_i = n_e = 2 \times 10^{19} \text{ m}^{-3}$, and flat temperatures $T_i = T_e = 1$ keV. A Maxwellian is also chosen for the unperturbed distribution function of the fast particles (deuterium ions). The fast particle temperature T_f is flat and the fast particle density is given by the expression:

$$n_f(s_{\text{pol}}) = n_{0f} \exp \left[- \frac{\Delta_{nf}}{L_{nf}} \tanh \left(\frac{s_{\text{pol}} - s_{nf}}{\Delta_{nf}} \right) \right] \quad (23)$$

with s_{pol} being the square root of the normalised poloidal flux, $s_{\text{nf}} = 0.5$ the position of the maximal value of $\kappa_{\text{nf}} = |\nabla n_f|/n_f$, $n_{0f} = 0.75 \times 10^{17} \text{ m}^{-3}$ the fast particle density at $s_{\text{pol}} = s_{\text{nf}}$, $\Delta_{\text{nf}} = 0.2$ the characteristic width of the density profile, and $L_{\text{nf}} = 0.3$ determining the strength of the fast particle density gradient.

In this configuration, we simulate the TAE with the toroidal mode number $n = -2$ and the dominant poloidal harmonics $m = 3$ and $m = 4$. This case is particularly difficult, since it corresponds to the so-called MHD limit at low perpendicular mode numbers, where the cancellation problem is most severe. It has been considered in Ref. [7] and is used here again to verify the pullback mitigation scheme.

In Figs. 1 and 2, the frequency and the growth rate of the TAE are shown, respectively, as functions of the fast-ion temperature. The result obtained with the pullback mitigation is compared with the MHD mitigation [7] simulations and with the electron-fluid scheme [20] simulations (the electron-fluid scheme is similar to Refs. [21, 22]). One sees that the agreement is excellent. Interestingly, the usual physical stabilization effect [23] due to the finite orbit width is rather weak here, in contrast to the moderate mode number simulations presented in Ref. [11]. Such a scaling is to be expected at the small dominant perpendicular mode numbers, considered in the present simulations.

We continue our numerical experiments with the pullback mitigation scheme in stellarator geometry. A magnetic geometry similar to the Large Helical Device (LHD) [24] is considered. The plasma is chosen to have $\beta_* = \mu_0 n_* T_* / B_*^2 = 0.0085$. Here n_* is the plasma density averaged over the entire plasma volume, $T_* = T_e(s = 0.5)$ with s being the normalised toroidal flux and $B_* = B(s = 0, \zeta = 0)$ with ζ being the toroidal angle. The plasma size is determined by the parameter $L_x = 900$ which is approximately the ratio $L_x \approx 2.2 r_a / \rho_s$ with r_a being the average minor radius of the non-axisymmetric device and $\rho_s = \sqrt{m_i T_*} / (e B_*)$ the characteristic ion sound gyroradius. Note that simulations at large values of L_x (small values of $\rho_* = \rho_s / r_a$) are particularly challenging since one can show that the cancellation problem scales as $\beta_* L_x^2$. The plasma density and temperatures profiles are defined as the functions of the normalised toroidal flux according to the expressions:

$$n_{(i,e)}(s) = n_0 \exp \left[- \frac{\Delta_n}{L_n} \tanh \left(\frac{s - s_0}{\Delta_n} \right) \right] \quad (24)$$

$$T_{(i,e)}(s) = T_0 \exp \left[- \frac{\Delta_{T(i,e)}}{L_{T(i,e)}} \tanh \left(\frac{s - s_0}{\Delta_{T(i,e)}} \right) \right] \quad (25)$$

with $s_0 = 0.5$, $1/L_n = 1.5$, $\Delta_n = 0.2$, $1/L_{T_i} = 3.5$, $\Delta_{T_i} = 0.2$, $1/L_{T_e} = 3.0$, and $\Delta_{T_e} = 0.2$.

The parameters n_0 and T_0 are determined by the plasma size L_x and its pressure β_* .

We consider an electromagnetic mode centered in the Fourier space around the poloidal mode number $m_0 = -35$ and the toroidal mode number $n_0 = -23$. This mode can be destabilised by finite ion temperature gradient, becoming the electromagnetic ITG mode. ‘Electromagnetic’ implies here that the gyrokinetic electromagnetic system of equations will be solved in the simulations at plasma β exceeding the hydrogen electron-to-ion mass ratio.

We start our simulations using the standard cancellation scheme [3, 5]. In Fig. 3, the time evolution of the mode is shown. One sees that it becomes strongly unstable within a few time steps. The Fourier spectrum is shown in Fig. 4: it is completely dominated by the noise at the edge of the Fourier window, caused by the cancellation problem. Finally, the radial pattern of the Fourier-decomposed quantity $\phi(s, \theta, \zeta_0)$ is shown in Fig. 5. Here, ϕ is the electrostatic potential, s is the normalised toroidal flux, θ is the poloidal angle and $\zeta_0 = 0$ is the particular (fixed) toroidal angle. Different lines correspond in Fig. 5 to different poloidal harmonics of $\phi(s, \theta, \zeta_0)$.

The cancellation problem can in stellarator geometry be somewhat alleviated with the MHD mitigation scheme, described in Ref. [7]. In Fig. 6, the time evolution is shown in the case when the MHD mitigation scheme is applied. One sees that the numerical instability sets in later in this case, but it is still present and disrupts the simulation. In Fig. 7, the Fourier spectrum of the mode is shown at the time of the instability onset, showing both the physical mode, still visible in the center of the Fourier window, accompanied by the wide-band noise signal appearing around the physical mode. A few time steps later, the noise dominates and the simulation dies. In Fig. 8, the radial pattern of the Fourier-decomposed $\phi(s, \theta, \zeta_0)$ is shown at the onset of the numerical instability. Again, the physical mode is still there and coexists with the distinct structure at the edge. This structure is caused by the cancellation problem and dominates the simulation after a few more time steps.

Finally, we describe simulations using the pullback mitigation. In Fig. 9, the time evolution of the electromagnetic ITG is shown. One sees now that the mode develops in a clean physical way. All parameters here are identical to those used for Figs. 3 and 6. The only difference is that the pullback mitigation has been switched on here. In Fig. 10, the Fourier spectrum is shown. One sees that the mode is numerically clean (cf. the structure with Figs. 4 or 7) and shows a ballooning-like structure, indicating importance of toroidicity in the case considered. In Figs. 11 and 12, the radial structure of the Fourier-decomposed

$\phi(s, \theta, \zeta_0)$ and its poloidal cross section are shown. One sees that the mode appears to be physical and ballooning-like in all these representations.

IV. CONCLUSIONS

In this paper, we have further developed the mixed-variable gyrokinetic formalism. In our previous work [7], the variables were determined by a particular form of Ohm's law. In the more general formulation presented here, such a limitation can be relaxed.

Using the mixed-variable formulation, we have proposed a new algorithm which can strongly mitigate the cancellation problem: pullback mitigation. The scheme follows the observation that the parallel dynamics is determined by the time derivative of the parallel magnetic potential whereas the cancellation problem is proportional to its value. Accumulating this value into the 'symplectic' part of the parallel magnetic potential makes it possible to minimise all terms that are relevant for the cancellation problem. Such a correction occurs at each time step in the course of a simulation, guaranteeing the smallness of the 'hamiltonian' residual. Note that pullback mitigation is not limited to the PIC framework.

We have verified the pullback mitigation approach in tokamak and stellarator geometries. In tokamak geometry, a Toroidal Alfvén Eigenmode with small mode numbers (the so-called MHD limit) has been simulated and compared with previous results. Very good agreement has been found. In stellarator geometry, the electromagnetic ITG mode has been simulated at a realistic ρ_* . It has been shown that the simulation becomes feasible, for the parameters considered, only when the pullback mitigation is used.

We believe that the approaches suggested in this paper and in Ref. [7] will greatly facilitate the electromagnetic simulations, both in tokamak and stellarator geometries. While only linear simulations have been considered here, our methods should also work in nonlinear regimes. We leave detailed study for future work.

ACKNOWLEDGEMENTS

We acknowledge the support of Per Helander for this work. We thank Jürgen Nührenberg for carefully reading the manuscript. Discussions on the cancellation problem during the workshop on "Modelling kinetic aspects of Global MHD Modes" organised by Egbert West-

erhof at the Lorentz Center in Leiden were very helpful. In particular, we acknowledge remarks by Arthur Peeters which provided an initial impulse for this paper. This work was carried out using the HELIOS supercomputer system at Computational Simulation Centre of International Fusion Energy Research Centre (IFERC-CSC), Aomori, Japan, under the Broader Approach collaboration between Euratom and Japan, implemented by Fusion for Energy and JAEA. Also, some simulations have been performed on the local cluster in Greifswald, where support of Henry Leyh is appreciated. The project has received funding from the Euratom research and training program 2014-2018.

-
- [1] Y. Chen and S. Parker, *Phys. Plasmas* **8**, 2095 (2001).
 - [2] A. Mishchenko, R. Hatzky, and A. Könies, *Phys. Plasmas* **11**, 5480 (2004).
 - [3] Y. Chen and S. Parker, *J. Comp. Phys* **189**, 463 (2003).
 - [4] A. Mishchenko, A. Könies, and R. Hatzky, in *Proc. of the Joint Varenna-Lausanne International Workshop* (Società Italiana di Fisica, Bologna, 2004).
 - [5] R. Hatzky, A. Könies, and A. Mishchenko, *J. Comp. Phys.* **225**, 568 (2007).
 - [6] J. Candy and R. E. Waltz, *J. Comp. Phys.* **186**, 545 (2003).
 - [7] A. Mishchenko, M. Cole, R. Kleiber, and A. Könies, *Phys. Plasmas* **21**, 052113 (2014).
 - [8] A. J. Brizard and T. S. Hahm, *Reviews of Modern Physics* **79**, 421 (2007).
 - [9] V. Kornilov, R. Kleiber, R. Hatzky, L. Villard, and G. Jost, *Phys. Plasmas* **11**, 3196 (2004).
 - [10] A. Mishchenko, R. Hatzky, and A. Könies, *Phys. Plasmas* **15**, 112106 (2008).
 - [11] A. Mishchenko, A. Könies, and R. Hatzky, *Phys. Plasmas* **16**, 082105 (2009).
 - [12] A. Mishchenko, A. Könies, and R. Hatzky, *Phys. Plasmas* **18**, 012504 (2011).
 - [13] A. Mishchenko and A. Zocco, *Phys. Plasmas* **19**, 122104 (2012).
 - [14] C. de Boor, *A Practical Guide to Splines* (Springer-Verlag, New York, 1978).
 - [15] K. Höllig, *Finite Element Methods with B-Splines* (Society for Industrial and Applied Mathematics, Philadelphia, 2003).
 - [16] M. Fivaz, S. Brunner, G. de Ridder, O. Sauter, T. M. Tran, J. Vaclavik, L. Villard, and K. Appert, *Comp. Phys. Commun.* **111**, 27 (1998).
 - [17] A. Mishchenko, A. Könies, and R. Hatzky, *Phys. Plasmas* **12**, 062305 (2005).
 - [18] W. W. Lee, *J. Comp. Phys.* **72**, 243 (1987).

- [19] R. Hatzky, T. M. Tran, A. Könies, R. Kleiber, and S. J. Allfrey, *Phys. Plasmas* **9**, 898 (2002).
- [20] M. Cole, A. Mishchenko, A. Könies, R. Kleiber, and M. Borchardt, *Phys. Plasmas* (accepted for publication in *Phys. Plasmas*).
- [21] Y. Chen and S. Parker, *Phys. Plasmas* **8**, 441 (2001).
- [22] Z. Lin and L. Chen, *Phys. Plasmas* **8**, 1447 (2001).
- [23] N. N. Gorelenkov, C. Z. Cheng, and G. Y. Fu, *Phys. Plasmas* **6**, 2802 (1999).
- [24] O. Motojima, N. Ohyabu, A. Komori, O. Kaneko, S. Masuzaki, A. Ejiri, M. Emoto, H. Funaba, M. Goto, K. Ida, H. Idei, S. Inagaki, N. Inoue, S. Kado, S. Kubo, R. Kumazawa, T. Minami, J. Miyazawa, T. Morisaki, S. Morita, S. Murakami, S. Muto, T. Mutoh, Y. Nagayama, Y. Nakamura, H. Nakanishi, K. Narihara, K. Nishimura, N. Noda, T. Kobuchi, S. Ohdachi, Y. Oka, M. Osakabe, T. Ozaki, B. J. Peterson, A. Sagara, S. Sakakibara, R. Sakamoto, H. Sasao, M. Sasao, K. Sato, M. Sato, T. Seki, T. Shimosuma, M. Shoji, H. Suzuki, Y. Takeiri, K. Tanaka, K. Toi, T. Tokuzawa, K. Tsumori, K. Tsuzuki, I. Yamada, S. Yamaguchi, M. Yokoyama, K. Y. Watanabe, T. Watari, Y. Hamada, K. Matsuoka, K. Murai, K. Ohkubo, I. Ohtake, M. Okamoto, S. Satoh, T. Satow, S. Sudo, S. Tanahashi, K. Yamazaki, M. Fujiwara, and A. Iiyoshi, *Nucl. Fusion* **43**, 1674 (2003).

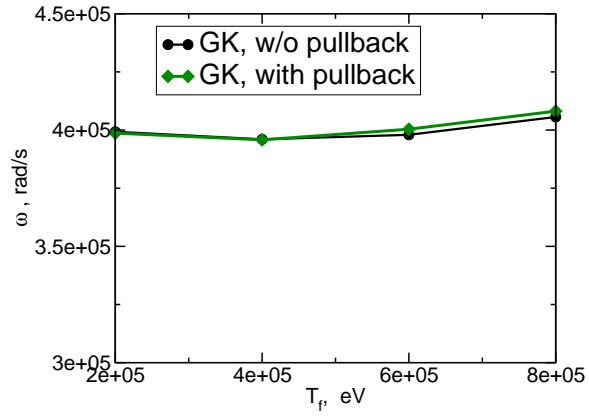


FIG. 1: (Color online) The frequency of the $n = -2$ TAE mode obtained with the pullback mitigation scheme compared with the MHD-mitigation [7].

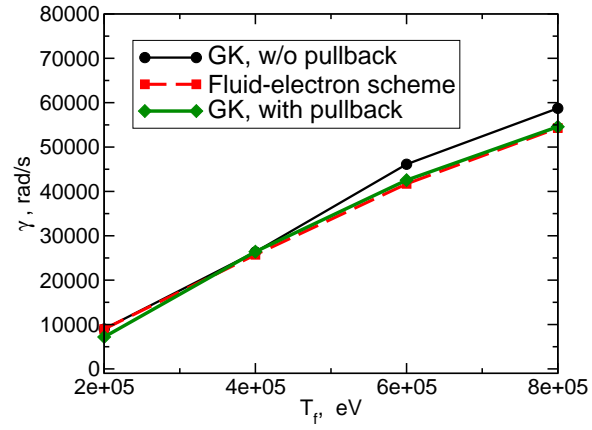


FIG. 2: (Color online) Growth rate of the $n = -2$ TAE mode obtained with the pullback mitigation scheme compared with the MHD-mitigation [7] and fluid-electron [20] schemes.

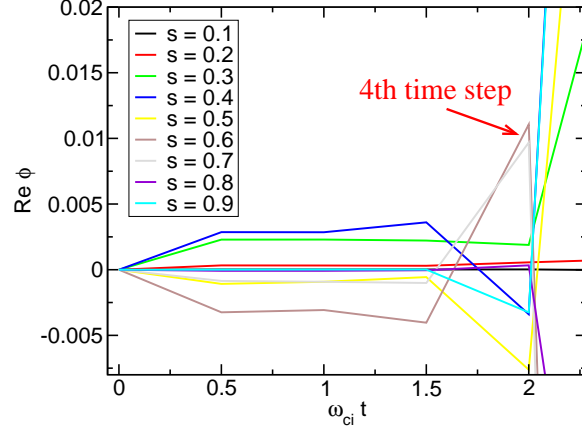


FIG. 3: (Color online) The time evolution of the electrostatic potential in LHD-like geometry is shown for the case of the standard cancellation scheme [3, 5] applied. The time step is $\omega_{ci} \Delta t = 0.5$. The time evolution is measured at different flux surfaces indicated on the figure. The potential is calculated at the toroidal angle $\zeta = 0$ and the poloidal angle $\theta = 0$. One sees that a severe numerical instability develops in this case within a few time steps.

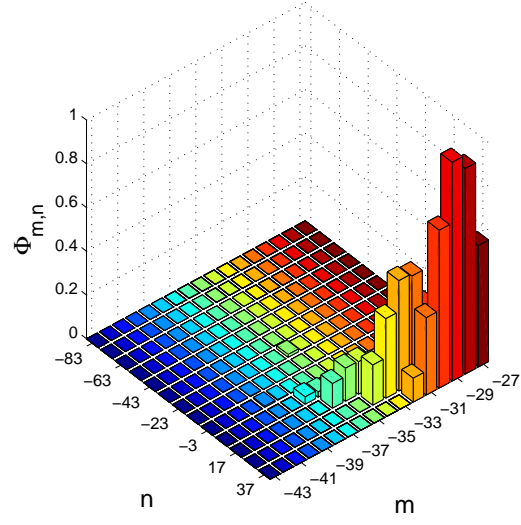


FIG. 4: (Color online) The Fourier window of the stellarator simulations is dominated by the modes at the edge within few time steps. The figure shown corresponds to the fourth time step. The standard cancellation scheme [3, 5] is used.

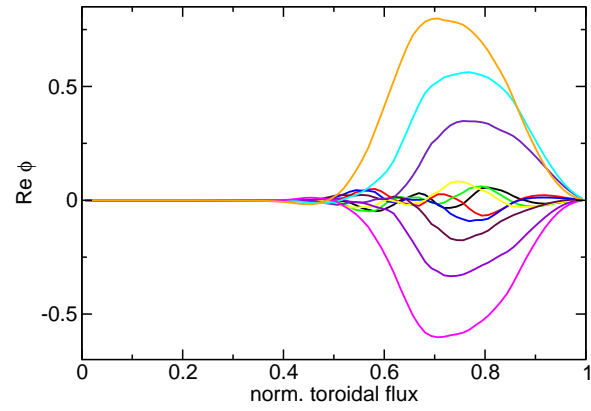


FIG. 5: (Color online) The radial pattern developing due to the severe numerical instability caused by the cancellation problem. The figure shown corresponds to the fourth time step. The standard cancellation scheme [3, 5] is used.

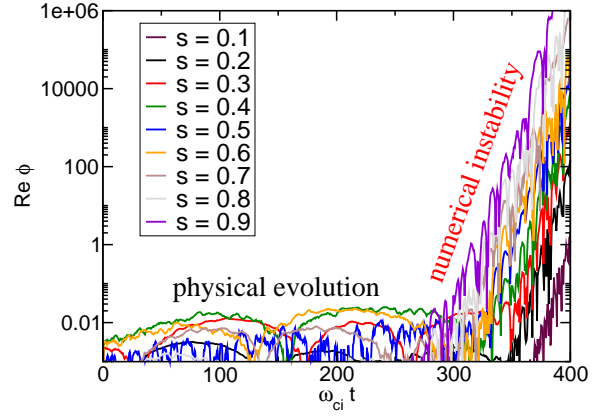


FIG. 6: (Color online) The time evolution of the electrostatic potential in the LHD-like configuration is shown for the case of the MHD-cancellation approach [7] applied. The numerical instability is mitigated using this approach, but can not be completely cured.

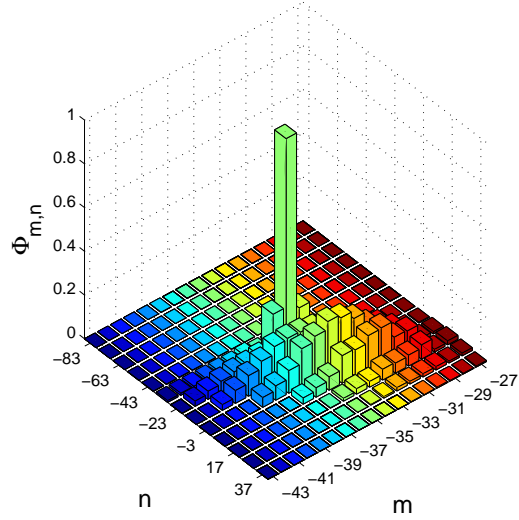


FIG. 7: (Color online) Onset of the numerical instability from Fig. 6, here shown in the Fourier window. The physical mode can still be seen in the center of the window. In addition, one sees a wide-band noise signal appearing. A few time steps later this part of the spectrum will dominate the mode completely: numerical instability develops.

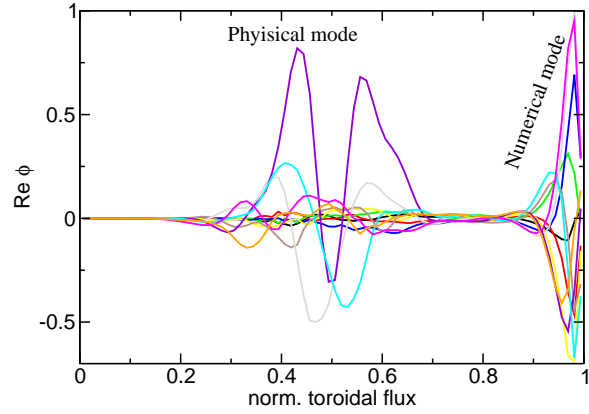


FIG. 8: (Color online) The radial structure developing during the numerical instability, see Fig. 6, caused by the cancellation problem. Onset of the numerical instability is shown. One sees both the physical mode still surviving and the noisy structure at the edge growing. A few time steps later, this noisy edge structure will completely dominate the radial pattern.

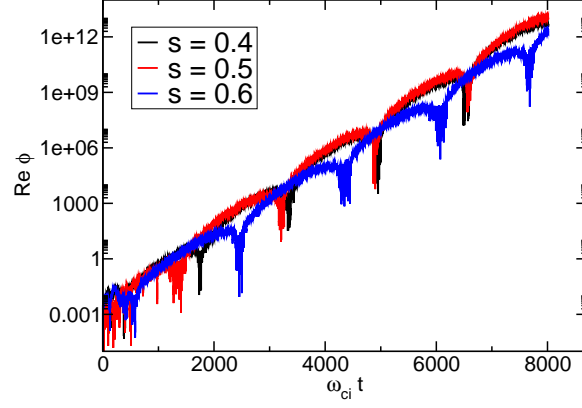


FIG. 9: (Color online) Numerically clean evolution of the physical mode obtained using the pullback mitigation approach. One sees that the mode (electromagnetic ITG) grows and has a finite frequency. All the numerical parameters coincide with the parameters used for Fig. 3. The only difference is the pullback mitigation, applied here.

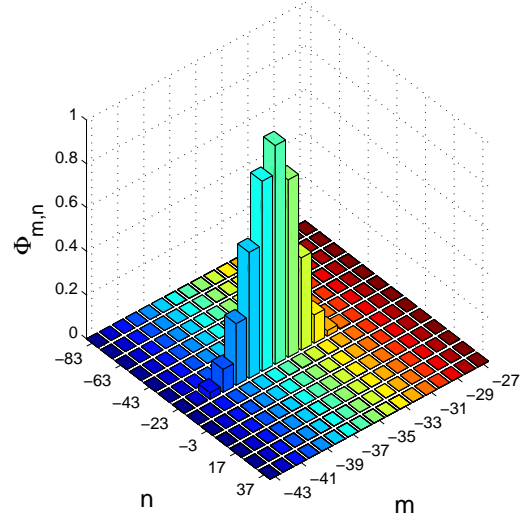


FIG. 10: (Color online) The physical, numerically clean Fourier spectrum of the electromagnetic ITG mode in LHD-like geometry. All the numerical parameters coincide with the parameters used for Fig. 4. The only difference is the pullback mitigation, applied here.

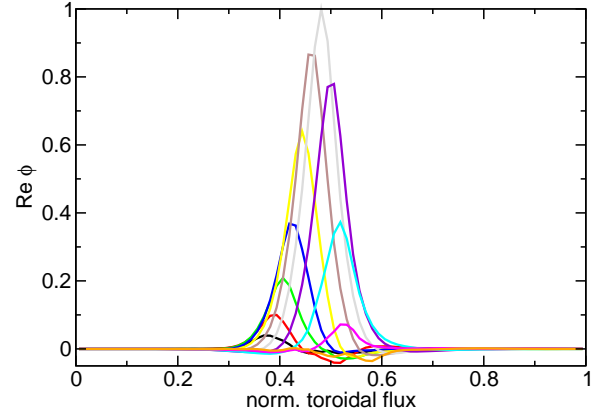


FIG. 11: (Color online) The radial pattern of the electromagnetic ITG mode. All the numerical parameters coincide with the parameters used for Fig. 5. The only difference is the pullback mitigation, applied here.

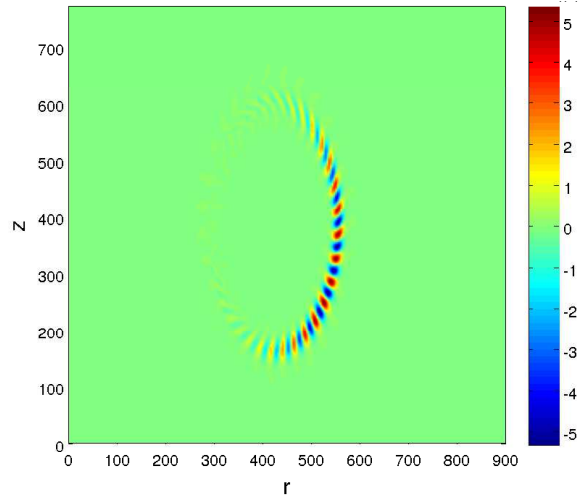


FIG. 12: (Color online) Electromagnetic ITG mode structure shown as a poloidal cross section at the toroidal angle $\zeta = 0$. Pullback mitigation of the cancellation problem has been applied.